Polymer Degradation and Stability 239 (2025) 111376

Contents lists available at ScienceDirect

Polymer Degradation and Stability

journal homepage: www.journals.elsevier.com/polymer-degradation-and-stability

Novel Si-MXene/PAPP hybrid system for high-performance flame-retardant polypropylene composites

Qinling Liu [a,b,c,d,#], Junhan Chu [a,b,c,d,#], Yuhui Xie [a,b,c,d,*], Zhaoyu Li [a,b,c,d], Feng Wu [a,b,c,d], Dong Feng [a,b,c,d], Yang Meng [a,b,c,d], Yi Mei [a,b,c,d], Delong Xie [a,b,c,d,*]

[a] Faculty of Chemical Engineering, Kunming University of Science and Technology, Kunming 650500, China
[b] Yunnan Provincial Key Laboratory of Energy Saving in Phosphorus Chemical Engineering and New Phosphorus Materials, Kunming 650500, China
[c] The International Joint Laboratory for Sustainable Polymers of Yunnan Province, Kunming 650500, China
[d] Yunnan Technological Innovation Center of Phosphorus Resources, Kunming 650600, China

ARTICLE INFO

Keywords:
Flame-retardant polypropylene
Si-modified MXene
Piperazine-modified APP
Synergistic flame retardancy

ABSTRACTS

The development of high-performance flame-retardant polypropylene (PP) composites is essential for enhancing fire safety across various industries. However, conventional intumescent flame retardant systems often suffer from poor char stability, weak condensed-phase protection, and insufficient gas-phase flame inhibition. To address these challenges, this study introduces a synergistic system combining Si-modified MXene (Si-MXene) and piperazine-modified ammonium polyphosphate (PAPP) to enhance the flame retardancy of PP composites. The piperazine modification of PAPP improves its compatibility with PP, facilitating uniform dispersion and enhancing its catalytic charring capability. Simultaneously, Si-modified MXene reinforces the char layer by promoting the formation of a highly graphitized and compact carbon structure, effectively blocking heat and oxygen transfer. As a result, the Si-MXene/PAPP system significantly reduces the peak heat release rate (PHRR) of PP by 52.6 % and total heat release (THR) by 35.4 %, while substantially improving thermal stability and char quality. Moreover, gas-phase analysis confirms that phosphorus radicals (P·, PO·) and non-flammable gases (NH_3, H_2O) scavenge combustion free radicals and dilute flammable volatiles, effectively suppressing flame propagation. This study provides a novel approach to developing high-efficiency flame-retardant PP composites, offering new insights into the synergistic mechanisms of MXene-based hybrid flame retardants and advancing the design of eco-friendly, high-performance polymeric materials for safety-critical applications.

1. Introduction

Polypropylene (PP) is a widely used general-purpose plastic due to its excellent processability, low cost, high chemical stability, and good mechanical properties. As a result, it is extensively utilized in various industries, including construction, electronics, electrical engineering, daily necessities, and medical devices, among others [1–5]. However, owing to the hydrocarbon-based structure of PP, it is inherently flammable and produces toxic gases upon combustion, which limits its applications in many safety-critical fields [6–8]. Therefore, there is a significant need to develop effective flame retardants for PP to enhance its fire safety and broaden its range of applications.

Currently, the two primary methods to impart fire-resistant properties to polymer matrices are chemical grafting and physical blending, both of which introduce flame-retardant elements into the polymer matrix [9,10]. From an economic perspective, physical blending is more commonly employed due to its cost-effectiveness. Conventional flame retardants, however, are often limited by their high loading requirements and relatively low flame-retardant efficiency. In contrast, intumescent flame retardant systems offer superior performance through the synergistic interaction of three key components: a gas source, an acid source, and a carbon source. During combustion, this system forms a dense intumescent char layer with a closed-cell structure. This carbonaceous residue layer not only effectively impedes oxygen diffusion and heat transfer but also significantly suppresses the release of combustible gases [11,12]. To optimize these advantages, researchers

* Corresponding authors at: Faculty of Chemical Engineering, Kunming University of Science and Technology, Kunming 650500, China.
E-mail addresses: yuhuixie@kust.edu.cn (Y. Xie), cedlxie@kust.edu.cn (D. Xie).
# Authors equally contributed to this paper.

https://doi.org/10.1016/j.polymdegradstab.2025.111376
Received 11 February 2025; Received in revised form 9 April 2025; Accepted 10 April 2025
Available online 11 April 2025

have focused on developing trifunctional integrated flame retardants. In particular, the construction of multifunctional synergistic flame-retardant systems using ammonium polyphosphate (APP) as a matrix material has emerged as a prominent research direction. APP inherently combines gas-source and acid-source properties, making it an ideal candidate for this purpose [13–18].

As a novel class of nitrogen-based carbon-forming agents, piperazines offer considerable advantages in flame-retardant systems. Compared to conventional polyol-based carbon sources, the nitrogen-rich heterocyclic structure of piperazine molecules enables a dual function during the pyrolysis process. This includes the release of inert gases through deamination reactions and the formation of highly graphitized carbon layers through aromatization reactions [19–21]. Gao et al. [22] synthesized a novel bio-based flame retardant, PHYPI, by reacting phytic acid with piperazine and applied it to PP. At a concentration of 18 wt % of PHYPI, the material achieved a V-0 rating and an increase in LOI from 18 % to 25 %.

However, conventional IFR systems often require a high loading to achieve adequate flame retardancy. At elevated loadings, the compatibility between the IFR and the polymer matrix decreases, which in turn can negatively impact the mechanical properties and flame retardancy efficiency [7,23,24]. It has been shown that incorporating inorganic nanofillers into the system can create a synergistic effect, enhancing flame retardancy, thermal stability, and mechanical properties, while simultaneously reducing the required IFR loading [25].

Since its discovery in 2011, MXene has attracted considerable attention as a promising class of two-dimensional materials. MXene exhibits metal-like electrical conductivity, tunable surface functional groups, and high mechanical strength. MXene is typically derived from MAX phases through selective etching of the A layer, with their general formula expressed as $M_{n+1}X_nT_x$, where M denotes an early transition metal (e.g., Ti, Zr, Cr), X stands for carbon or nitrogen, A represents the third- or fourth-group elements, and T corresponds to surface functional groups (e.g., -O, -OH, -F, and -Cl) formed after etching [26–28]. Due to its unique layered structure and excellent conductivity, MXene shows great potential in a range of applications, including electromagnetic interference (EMI) shielding [29,30], sensors [31,32], and photocatalysis [33,34]. Additionally, MXene has been explored as a synergistic flame retardant and capacitance enhancer in flame-retardant systems. For example, Sheng et al. [35] prepared PAM composite aerogels from PVA, APP, and MXene via freeze-drying. They found that at a 2 wt % MXene addition, the LOI of PAM increased to 42 %, surpassing the V-0 classification.

However, substantial evidence suggests that MXene nanosheets tend to agglomerate and reaccumulate during processing, leading to poor dispersion and oxidation, which can negatively affect the flame retardant performance. Therefore, surface modification of MXene is essential to improve its dispersion and flame retardancy [10,36,37]. Xie's research group has extensively studied the flame retardancy of MXene. In their work on MXene-based flame-retardant thermoplastic polyurethane (TPU) materials, they developed a series of novel functionalized MXene materials, including phosphorylated chitosan-functionalized MXene (PCS-MXene) [38], black phosphazene-MXene@polydopamine (BP-MXene@PDA) nanohybrid materials [39], and MXene-based intumescent flame retardant (PB-MXene) [40]. These materials demonstrated excellent flame retardant performance in TPU, with reductions of 66.7 %, 64.2 %, and 72.6 % in peak heat release rate (pHRR), and reductions of 21.0 %, 27.3 %, and 25.4 % in total heat release (THR), respectively, compared to pure TPU. Furthermore, MXene-functionalized polyphosphononitrile (MXene-PZN) exhibited outstanding flame-retardant properties when applied to epoxy resin [41].

Despite the well-documented advantages of MXene, its use as a flame retardant in PP remains underexplored. In this study, we aim to modify MXene with γ-aminopropyltriethoxysilane (KH-550) to obtain silicone-modified MXene, i.e., Si-MXene, addressing the issue of MXene's susceptibility to oxidation and improving its dispersion within the polymer matrix. We then combine Si-MXene with piperazine-modified ammonium polyphosphate (PAPP) to form a novel flame-retardant system. The flame retardancy and thermal stability of the PP composites are evaluated using cone calorimeter and thermogravimetric analysis (TGA), respectively, and the synergistic effects between the two components are explored. Finally, a potential mechanism for the enhanced flame retardancy of the composite is proposed and discussed.

2. Experimental section

2.1. Materials

MAX (Ti_3AlC_2, 98 % purity) was obtained from Jilin Yiyi Science and Technology Co. Ltd. The following reagents were sourced from Shanghai Aladdin Biochemical Technology Co. Ltd.: lithium fluoride (AR), lithium chloride (AR), dimethyl sulfoxide (AR), KH-550 (AR), and anhydrous piperazine (AR). Hydrochloric acid (AR) and anhydrous ethanol (AR) were purchased from Chengdu Cologne Chemical Co. Ltd. Acetic acid (AR) was obtained from Tianjin Windship Chemical Reagent Technology Co. Ltd. Ammonium polyphosphate was supplied by Kline Chemicals Ltd., while polypropylene (PP) was provided by Beijing Yanshan Petrochemical Co. Ltd.

2.2. Preparation of piperazine-modified ammonium polyphosphate

The preparation of PAPP begins with the preparation of a solvent mixture consisting of ethanol and deionized water (700 mL:40 mL), which is transferred to a round-bottom three-neck flask equipped with the necessary devices. The solution is purged with nitrogen and stirred for 30 min. Anhydrous piperazine (43 g) is then added to the flask, and the mixture is stirred until fully dissolved and homogeneous. Following this, 100 g of ammonium polyphosphate (APP) is dispersed evenly into the flask, along with an appropriate amount of anhydrous ethanol. The reaction temperature is set to 90°C. After the reaction time, the pH value reaches approximately 8–9 within 10 min, indicating the completion of the reaction. The mixture is then cooled to room temperature, and the resulting white solid is washed repeatedly with anhydrous ethanol to remove impurities. Finally, the product is placed in a vacuum drying oven until a constant weight is achieved. The whole process was illustrated in Figure S1.

2.3. Synthesis of Si-MXene

2.2.1. Etching of MXene nanosheets

In the first step, 2 g of MAX powder is gradually added to a Teflon centrifuge tube containing 40 mL of 3 M LiF and 9 M HCl. The solution is stirred uniformly at 38°C for 48 h. After completion of the reaction, the solution is washed with HCl and LiCl, followed by several rinses with deionized water until the pH of the solution becomes neutral. The resulting colloidal solution is then dispersed in a round-bottom flask with deionized water, and the solution is purged with nitrogen to protect it from oxidation. After nitrogen purging, the sample undergoes sonication at room temperature for one hour. Subsequently, the solution is centrifuged at 3500 rpm for one hour, and the supernatant is stored in a sealed container for refrigeration or freeze-drying for further treatment. The illustration of the preparation process was shown in Figure S1.

2.2.2. Silicon modification of MXene

The prepared MXene nanosheets are dispersed in 45 mL of dimethyl sulfoxide (DMSO) solution and sonicated for 30 min per gram of material. The suspension is then magnetically stirred for 48 h under a nitrogen-protected atmosphere. Afterward, the mixture is centrifuged at 12,000 rpm for 15 min and washed with deionized water to remove excess solvent. The resulting products are freeze-dried to obtain hydroxylated MXene (MXene-OH). 1 g of MXene-OH is sonicated in 50 mL

of a water/ethanol (10/90 wt. %) mixture for 1 hour, and then transferred to a three-necked flask. An equal mass of KH-550 is then added to 50 mL of the water/ethanol mixture, and the pH is adjusted to 4.5 with glacial acetic acid. The mixture is pre-hydrolyzed in the solvent for 2 h. After hydrolysis, the solution is added dropwise to the three-necked flask using a peristaltic pump. The flask is then mechanically stirred under nitrogen bubbling for 7 h at 30°C. Upon completion of the reaction, the remaining KH-550 is removed by washing with a 50 wt. % ethanol solution at 8000 rpm. The product was then subjected to a drying process in a vacuum freeze-drying oven, with the objective of obtaining the silanised MXene, i.e., Si-MXene. The illustration of the preparation process was shown in Figure S1.

2.4. Preparation of Si-MXene/PAPP/PP composites

Si-MXene powder and PAPP are combined through a melt mixing process using a rubber and plastic mixing machine (LH300, Shanghai Kechuang Rubber & Plastic Machinery Co., Ltd.) set at 175°C with a rotation speed of 50 r/min for 20 min. Afterward, the fused PP is cut into small pieces using a plate vulcanization instrument (XY-25; Jiangdu District Xuanyu Experimental Machinery Factory) at 175°C, with temperatures of 20°C and pressures of 10 MPa and 5 MPa, following 300 s of hot pressing and 120 s of cold pressing treatment. Table 1 lists the components of the Si-MXene/PAPP/PP composite, and the synthesis route is illustrated in Fig. 1.

2.5. Characterizations

2.5.1. Morphological and structural analysis

The chemical structures of the flame retardants and residual carbon were characterized using a Tensor-II Fourier infrared spectrometer (Bruker, USA), with a wavelength range of 400–4000 cm^{-1}. The crystalline structures of the nanomaterials and residual carbon were analyzed using X-Ray Powder Diffraction (XRD) on an X/pert-3 X-ray diffractometer (Philips, Netherlands), employing Kα radiation from an Al target at a scanning speed of 10°/min in the range of 5°–85° The chemical bonding and elemental composition of the nanomaterials and residual carbon were investigated by X-ray photoelectron spectroscopy (XPS), using a Thermo Scientific K-Alpha instrument. The morphology of the nanomaterials was observed using a TESCAN MIRA LMS scanning electron microscope (SEM), while the elemental distribution maps of nanomaterials were obtained via the Energy-Dispersive X-ray Spectroscopy (EDS). The microscopic morphology of MXene and other samples was analyzed using a Thermo Fisher Talos F200S G2 transmission electron microscope (TEM). The thickness of the MXene nanosheets was measured using a Bruker Dimension Icon atomic force microscope (AFM).

2.5.2. Measurement of thermal stability, flame retardancy and mechanical properties

The thermal stability of the flame retardants and PP composites was assessed through TGA using a NETZSCH STA 449 F3 instrument. The samples were heated in a nitrogen atmosphere at a flow rate of 50 mL/min, with a temperature increase rate of 20°C/min, and the temperature range was 40°C–800°C. The flame retardancy of the composites was evaluated using a PHINIX cone calorimeter in accordance with ISO 5660–1, with a heat flux of 50 kW/m^2 for combustion experiments. The limit oxygen index (LOI) was determined using a COI-type tester supplied by Modis Combustion Technology Co. Ltd., in accordance with GB/T 2406–2–2009. The vertical combustion test was conducted using a CZF-6 horizontal and vertical combustion tester (Nanjing Jiangning Analytical Instrument Co., Ltd.), in line with GB/T 2408–2021. The mechanical properties of the composites were evaluated according to GB/T 1043–93 using an ETM104B instrument (Shenzhen Wanmei). The tensile rate was set at 50 mm/min. Thermogravimetry-Fourier Transform Infrared Spectroscopy (TG-FTIR) was performed using a Tensor-II Fourier infrared spectrometer in conjunction with a NETZSCH STA449F3 TGA thermogravimetric analyzer in a nitrogen atmosphere at a flow rate of 100 mL/min. The temperature range for the analysis was 40°C–800°C, with a temperature increase rate of 10°C/min.

Table 1
Composition of PP/PAPP/Si-MXene composite components.

Samples	Component		
	PP(wt %)	PAPP(wt %)	Si-MXene(wt %)
PP	100	–	–
PP/10PAPP	90	10	–
PP/9.5PAPP/0.5Si-MXene	90	9.5	0.5
PP/9PAPP/1Si-MXene	90	9	1
PP/8.5PAPP/1.5Si-MXene	90	8.5	1.5
PP/8PAPP/2Si-MXene	90	8	2

3 Results and discussion

3.1. Characterization of PAPP/Si-MXene/PP composites

3.1.1. Structural characterization of PAPP

The FTIR spectra of APP and PAPP, as shown in Fig. 2, reveal the presence of characteristic peaks corresponding to both APP and PAPP. In addition to the peaks observed for APP, two new absorption peaks at 2780 cm^{-1} and 2643 cm^{-1} are present, which can be attributed to the vibrational peaks of -CH_2 and -NH_2^+ groups, respectively [42]. The appearance of these peaks suggests a reaction between APP and piperazine, resulting in the formation of a new bond, specifically the piperazine salt (-$NH_2^+$$^-$O-P-). The main stretching vibrational peaks of P-O-C, P-O, and C-N were observed in the range of 800–1500 cm^{-1}. The stretching vibration peak at 3400–3000 cm^{-1} corresponds to the NH_4^+ vibration [43]. The presence of the NH_4^+ peak indicates the persistence of ammonium ions (from the precursor material) in the PAPP product.

3.1.2. Structural characterization of Si-MXene

The morphologies of MAX and MXene were observed using SEM. The SEM images of MAX before and after etching are shown in Fig. 3a and b, respectively. MAX exhibits a distinct massive morphology, while MXene demonstrates a sparse accordion-like lamellar structure after etching of the Al layer. This indicates successful etching of MXene. Further insights into the crystal structure were obtained through XRD analysis, and the results are presented in Fig. 3c. The XRD pattern of MAX shows multiple distinct peaks, with peak (002) representing the characteristic peak of MAX and peak (104) corresponding to the presence of Al in the MAX phase. After etching, the characteristic peak (002) of MXene shifts to a lower angle, from 9.48° to 6.51°, indicating a reduction in the nanosheet layer thickness and an increase in the width of peak (002). This shift can be attributed to the insertion of functional groups such as OH, -F, and -Cl during the etching process, which increases the interlayer spacing [44] . This also facilitates the removal of impurities between the layers. The TEM image of MXene in Fig. 3d reveals a typical lamellar structure, showing the synthesized ultra-thin nanosheets. Additionally, AFM images in Fig. 3(e–f) reveal that the average thickness of the MXene nanosheets is approximately 2 nm. These results confirm the successful synthesis of MXene nanosheets.

To demonstrate the effectiveness of MXene modification, FTIR, XPS, and XRD analyses were conducted on the Si-MXene. In the FTIR spectrum (Fig. 4a), the absorption peak at 565 cm^{-1} is attributed to the Ti-O bond, a defining feature of MXene. The peaks at 1090 cm^{-1} correspond to the Si-O-Si bond, providing preliminary evidence of successful modification. The peaks observed at approximately 947 cm^{-1} can be attributed to Si-O-Ti bonds. The -OH peak of the original MXene at 3400 cm^{-1} is no longer present after modification, indicating that the majority of -OH groups on MXene have reacted with the silane coupling agent to form Si-O-Si and Si-O-Ti bonds. This suggests that the modification process

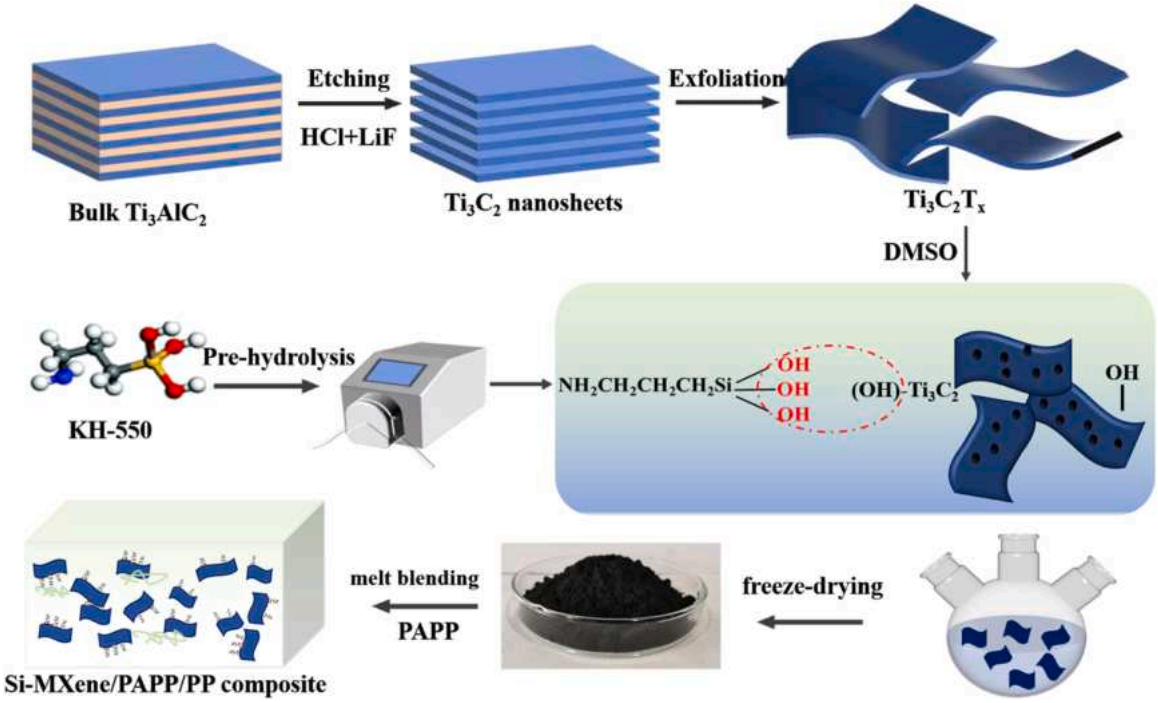

Fig. 1. Synthesis route of Si-MXene/PAPP/PP composites.

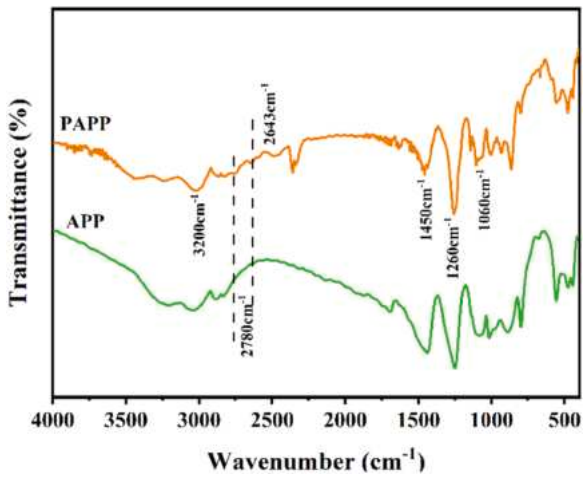

Fig. 2. FTIR spectra of APP and PAPP.

effectively involved a chemical interaction between MXene and the silane agent, leading to the formation of stable chemical bonds.

The formation of the Si-MXene bond was further examined through XPS analysis. The high-resolution spectra of Si 2p and Ti 2p are shown in Fig. 4b and c, respectively. In the Si 2p spectrum, peaks at 102, 102.6, and 103.5 eV correspond to Si-O-C, Si-O-Si, and Si-O-Ti bonds, respectively. In the Ti 2p spectrum, a new Ti-O-Si bond appears at 439.3 eV, along with changes in the intensity and position of other peaks compared to the initial MXene. The reduction in binding energy is attributed to the presence of KH-550 molecular chains in the MXene material. The peak at 465.5 eV corresponds to TiO_2, indicating that a small degree of oxidation remains. The XRD pattern in Fig. 4d shows that the (002) characteristic peak of Si-MXene retains its position but shifts to a lower angle, reaching approximately 5°, indicating that the interlayer spacing of MXene further expanded with the introduction of the Si molecular chain, while the layered structure remained intact.

TGA of raw and modified materials under a nitrogen atmosphere is shown in Fig. 4(e–f), and the corre sponding data is collected in Table 2. KH-550 shows rapid degradation at 800°C with a residual carbon content of 8.09 %. MAX exhibits excellent thermal stability, with negligible weight loss up to 800°C. For MXene, a weight loss of 5 % ($T_{5\,\%}$) occurs at 250.3°C, with a further mass loss of 9.43 % observed at 800°C, attributed to the decomposition of surface groups such as -F, -OH, and -O. Si-MXene shows a weight loss of 20.22 %, which is higher than that of MXene, due to the decomposition of grafted silicon. Despite this, the modified MXene demonstrates significant thermal stability. As shown in Fig. 5, the modified MXene retains its characteristic layered structure. The incorporation of KH-550 results in thickened nanosheet layers and a curled morphology. EDX analysis confirms the uniform distribution of elements, including C, Ti, Si, and O, throughout the sample. These findings collectively validate the successful chemical modification of MXene.

3.1.3. *Structural characterization PAPP/Si-MXene/PP composites*

Fig. 6 shows the SEM cross-sections of pure PP and MXene-based PP composites. As observed in Fig. 6 a1 & a2, the internal structure of pure PP is relatively smooth, exhibiting only limited pleat-like patterns. When single PAPP is added to the composite, a coarser fracture surface is observed, as shown in Fig. 6 **b1 & b2**, indicating a stronger interface interaction between them. Additionally, a comparison of the cross-sectional SEM images of PP/10APP and PP/10PAPP samples, as shown in **Figure S3**, confirms that piperazine modification enhances the dispersion efficiency of APP within the polypropylene matrix. In contrast, when part of the PAPP load is replaced by Si-MXene, the fracture surface becomes smoother, as seen in Fig. 6 **c1 & c2**. This suggests that Si-MXene enhances the compatibility between the flame retardant and the PP matrix. The hydrogen bonding between the chain segments of Si-MXene and the PP matrix contributes to this improvement, with the incorporation of nanomaterials enhancing the mechanical properties of the composite.

Fig. 6 shows the cross-sectional SEM images and elemental distribution of the composites. SEM-EDS analysis was employed to investigate the synergistic distribution patterns of the multicomponent fillers in the polypropylene matrix. As seen in Figs. 6(d-f), characteristic elemental

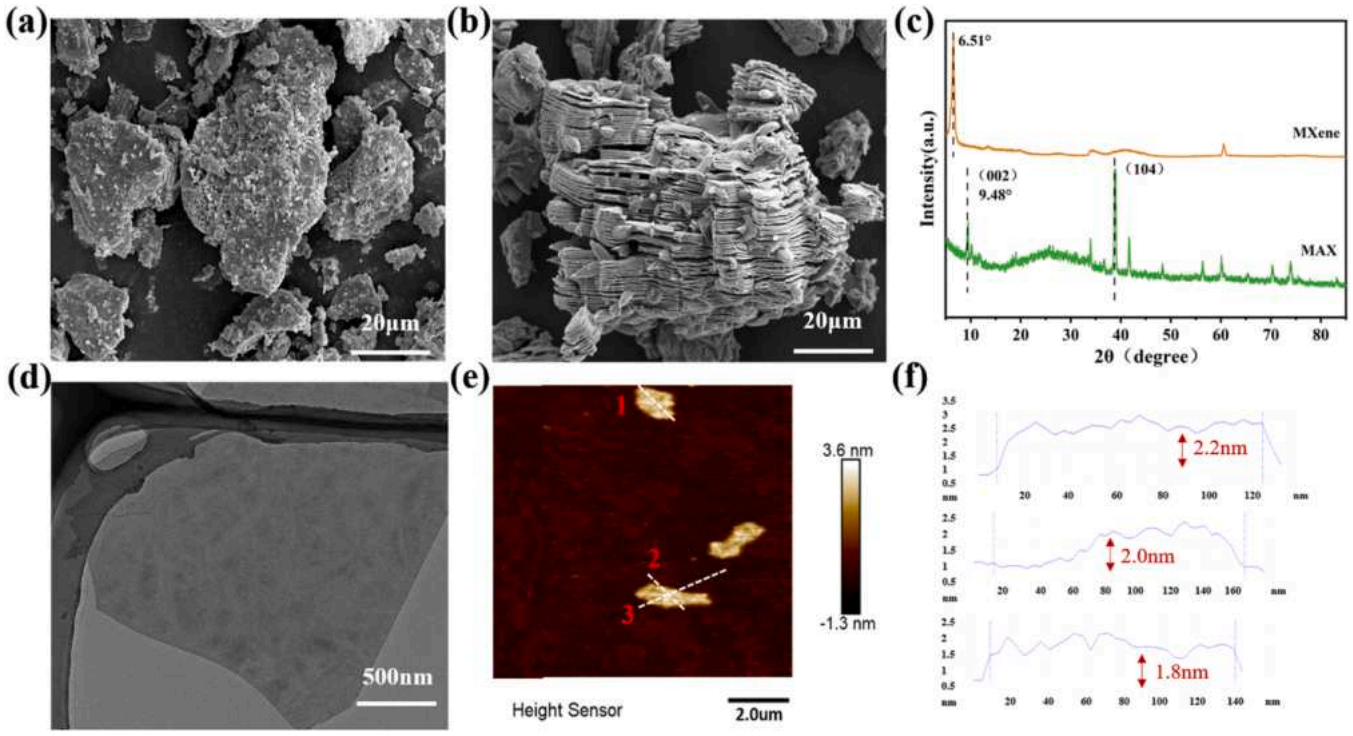

Fig. 3. SEM images of (a) MAX and (b) MXene; (c) XRD pattern analysis of MAX and MXene; (d) TEM image of MXene; (e–f) AFM images of MXene, with corresponding height profile.

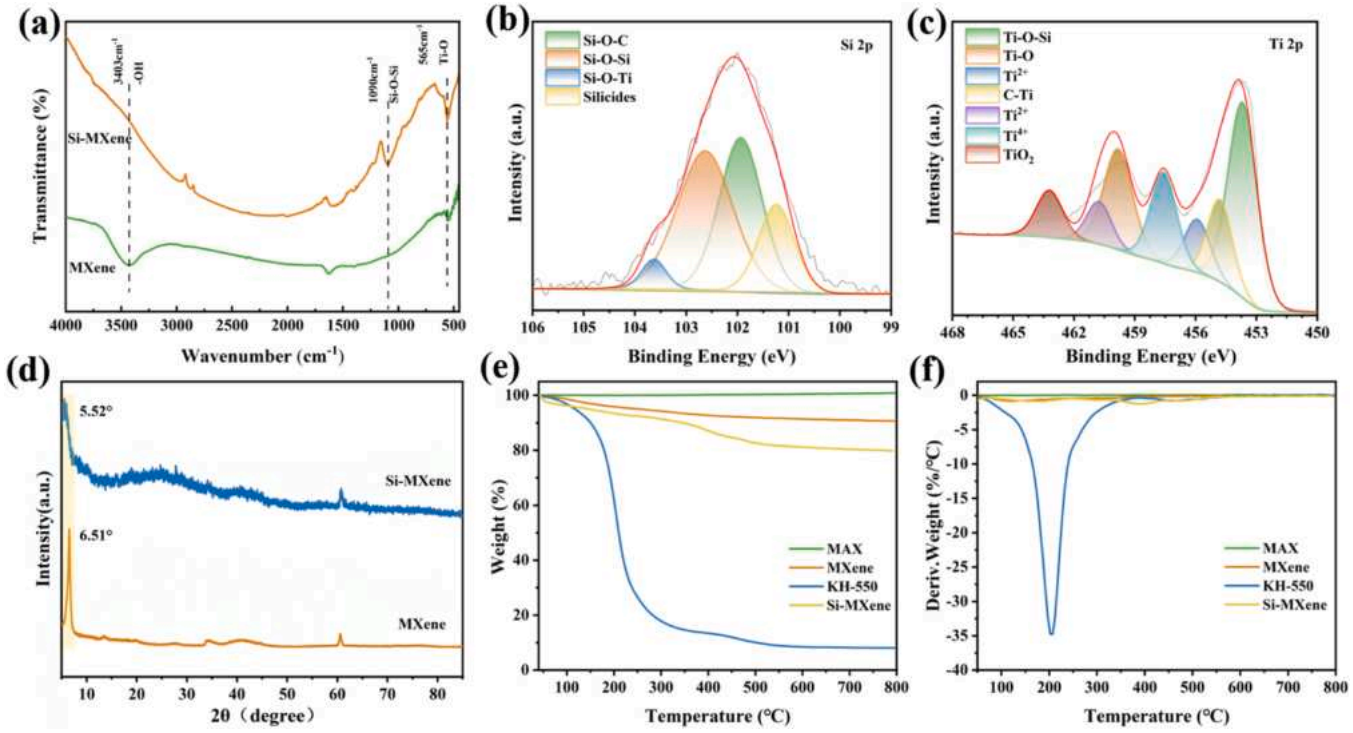

Fig. 4. (a) FTIR spectra of MXene and Si-MXene; (b–c) high-resolution Ti 2p and Si 2p XPS spectra of Si-MXene; (d) XRD patterns; (e-f) TGA and DTG curves of MAX, MXene, KH-550, and Si-MXene under nitrogen atmosphere.

signals corresponding to each component were detected in all three samples. Notably, while localized enrichment of phosphorus (P) was observed in all systems, the PP/9.5PAPP/0.5Si-MXene system, incorporating Si-MXene, exhibited a notable improvement in the uniformity of P distribution. Compared to the unmodified PP/9.5PAPP/0.5MXene system, the PP/9.5PAPP/0.5Si-MXene composite demonstrated enhanced dispersion of both Ti and P elements, with a more pronounced improvement in Ti element dispersion. These results suggest that the introduction of Si-MXene not only enhances the dispersion of MXene nanosheets in the polymer matrix through surface modification, but also

Table 2
TGA data of MAX, MXene, KH-550, and Si-MXene under nitrogen atmosphere.

Samples	$T_{5\ \%}$ (°C)	$T_{50\ \%}$ (°C)	T_{max} (°C)	$T_{90\ \%}$ (°C)	$Char_{800}$ (%)
MAX	–	–	–	–	100.78
MXene	230.2	–	–	–	90.57
KH-550	116.8	209.4	203.9	502.3	8.09
Si-MXene	145.9	–	–	–	79.78

helps improve the dispersion of PAPP to a certain extent.

3.2. Properties evaluation of PAPP/Si-MXene/PP composites

3.2.1. Mechanical properties of composite materials

The mechanical properties of PP and its composites were evaluated, as they significantly impact the material's potential applications in engineering. Fig. 7 shows the stress-strain curves and elongation at break. Pure PP exhibits a tensile strength of 22.3 MPa and an elongation at break of 29.9 %. The addition of 10 wt % PAPP alone causes a significant reduction in the mechanical properties, with tensile strength dropping to 14.8 MPa and elongation at break to 22.1 %. This decline is consistent with the observed poor dispersion of PAPP in the matrix, as previously discussed. In contrast, the addition of Si-MXene notably improves the elongation at break. For example, the elongation at break of the 9.5PAPP/0.5Si-MXene/PP composite increased to 62.9 %, a 52.4 % increase compared to pure PP, and a 64.9 % increase compared to 10PAPP/PP. However, increasing Si-MXene content to 2 wt % resulted in a decrease in elongation at break, likely due to aggregation at higher concentrations.

3.2.2. Thermal stability of composite materials

The TGA results are shown in Fig. 8, and the relevant data are summarized in Table 3. The thermal decomposition of each formulation follows a similar trend in the TGA curve, with minimal weight loss observed below 400 °C. The addition of PAPP significantly increases $T_{5\ \%}$, along with a substantial increase in carbon residue, from 0.15 % for pure PP to 4.84 %. This effect can be attributed to the release of phosphoric acid and related phosphorus compounds from PAPP during heating, which forms a protective coating on the substrate surface, preventing further decomposition of the matrix. The introduction of Si-MXene notably raises the decomposition temperature of the PP composite. Specifically, adding 0.5 wt % Si-MXene and 9.5 wt % PAPP results in the highest $T_{5\ \%}$, which increases from 398.5 °C for pure PP to 416.1 °C for the PP/9.5PAPP/0.5Si-MXene composite. Additionally, both $T_{5\ \%}$ and carbon residue are significantly higher than those of the PAPP-only composite. These findings indicate that Si-MXene provides a beneficial synergistic effect with PAPP to enhance the thermal stability of PP composite. Furthermore, at 800 °C, pure PP leaves only 0.15 % residual mass. However, with the addition of flame retardants, the carbon residue of the composite materials increases to 4.84 %, 5.05 %, 5.24 %, 5.56 %, and 4.17 %, respectively. The MXene-based phosphate-containing intumescent flame-retardant system exhibits enhanced carbon formation capacity compared to that of PAPP alone, although the loading amount of Si-MXene was limited to be <2 wt. %. The reason could be that the titanium dioxide (TiO_2) formed from MXene degradation also facilitates cross-linking and carbonization of PAPP and PP, thus forming a high-quality expansion barrier layer [38]. In addition, the improved dispersion of modified MXene in the substrate can also enhance the interaction between the flame retardant and the substrate, promoting the formation of a more stable, cross-linked carbon layer.

3.2.3. Flame-retardant properties of composite materials

A cone calorimeter (CC), a laboratory-scale combustion test instrument, simulates the combustion behavior of materials in real-world fire scenarios. The results of the CC test, shown in Fig. 9 (a-d) and Table 4, provide detailed data on the combustion behavior of the composite materials. Fig. 9(a-b) present the heat release rate (HRR) and total heat release (THR) curves for PP composites during combustion. Pure PP exhibits vigorous combustion, with peak heat release rate (PHRR) and THR values of 1113.3 kW/m^2 and 122.4 MJ/m^2, respectively. In contrast, the addition of PAPP reduces the ignition time, significantly lowering the PHRR to 636.8 kW/m^2 and THR to 101.1 MJ/m^2. Additionally, the combustion time is prolonged. Further, the inclusion of Si-MXene causes a shift in the HRR curve from a single-peak to a bimodal or multi-peak combustion pattern. The first peak occurs around 130 s, likely due to the strengthening of the carbon layer by the nanomaterials. While the carbon layer protects the substrate, combustion continues beneath the layer, eventually leading to its rupture and the emergence of second peak [45]. The addition of 0.5 wt % Si-MXene results in a 52.6 % reduction in PHRR and a 35.4 % reduction in THR compared to pure PP. While compared to the PP/10PAPP composite, PHRR and THR of PP/9.5PAPP/0.5SiMXene composite decrease by 17.2 % and 21.8 %, respectively.

One of the main concerns in polymer combustion is the release of toxic gases such as CO and CO_2, which pose significant risks to human health and safety. Therefore, reducing gas emissions is crucial for improving the safety of flame-retardant materials. Figs. 9(c-d) shows the variation of CO_2 and CO volume fractions in flue gas for PP composites. The results indicate that adding even a small amount of Si-MXene to PAPP significantly reduces the concentration of CO and CO_2 compared to pure PP and PAPP alone. This suggests that nanofillers play a key role in reducing smoke release. The synergistic effect of Si-MXene and PAPP improves flame retardancy, decreasing the thermal decomposition products and harmful gases during combustion [46]. Furthermore,

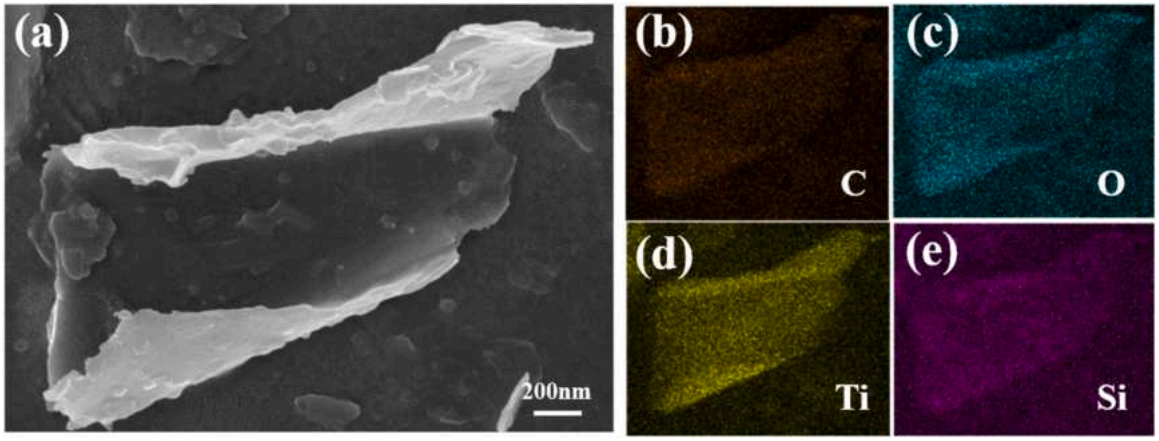

Fig. 5. (a) SEM images of Si-MXene; (b-e) EDX elemental mapping of Si-MXene.

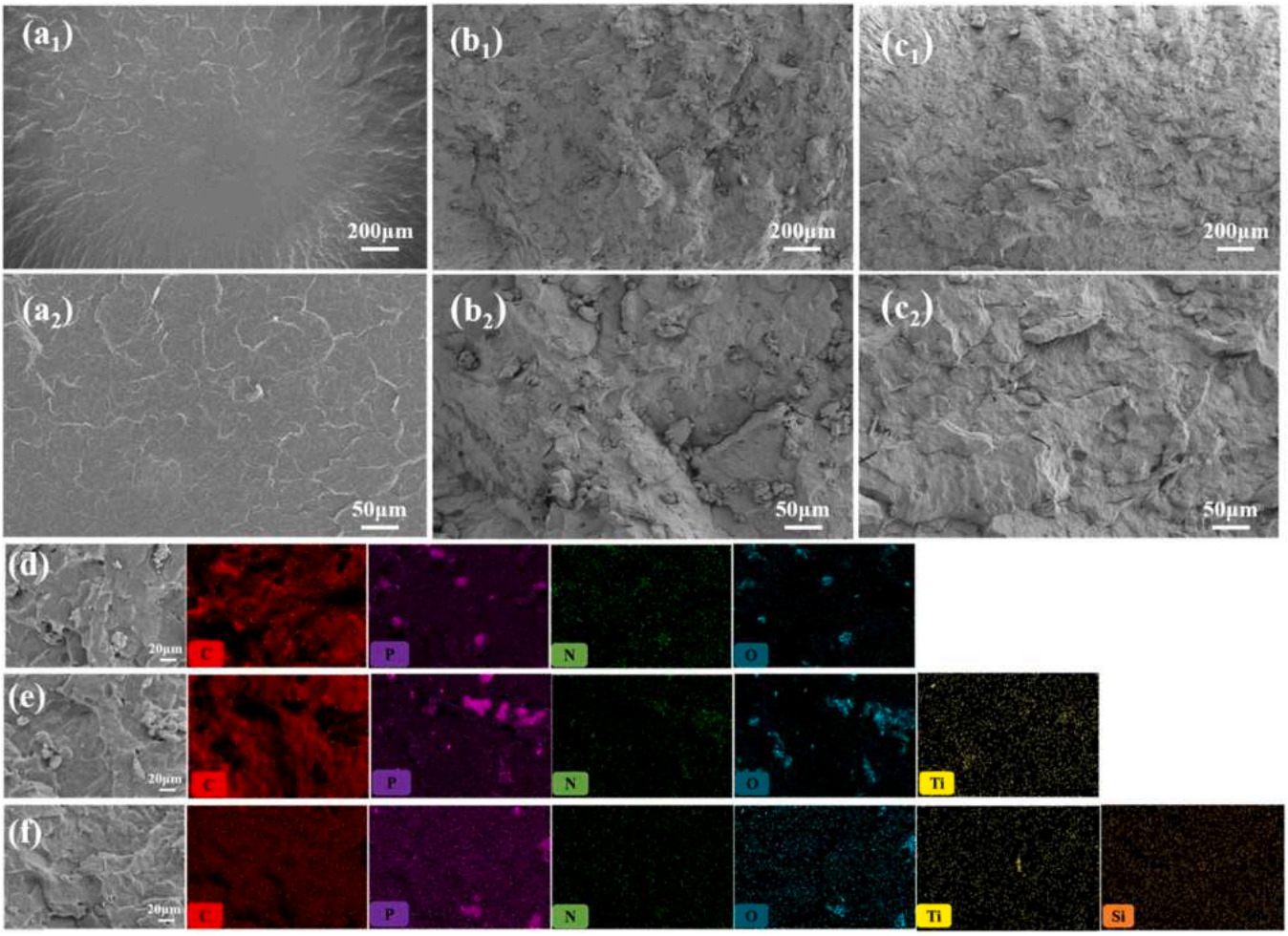

Fig. 6. (a1-a2) Cross-sectional SEM of pure PP; (b1-b2) SEM image of PP/10PAPP; (c1-c2) SEM image of PP/9.5PAPP/0.5Si-MXene; (d) Distribution of C, P, N, and O elements in PP/10PAPP; (e) Distribution of C, P, N, O, and Ti elements in PP/9.5PAPP/0.5MXene; (f) Distribution of C, P, N, O, Ti and Si elements in PP/9.5PAPP/0.5Si-Mxene.

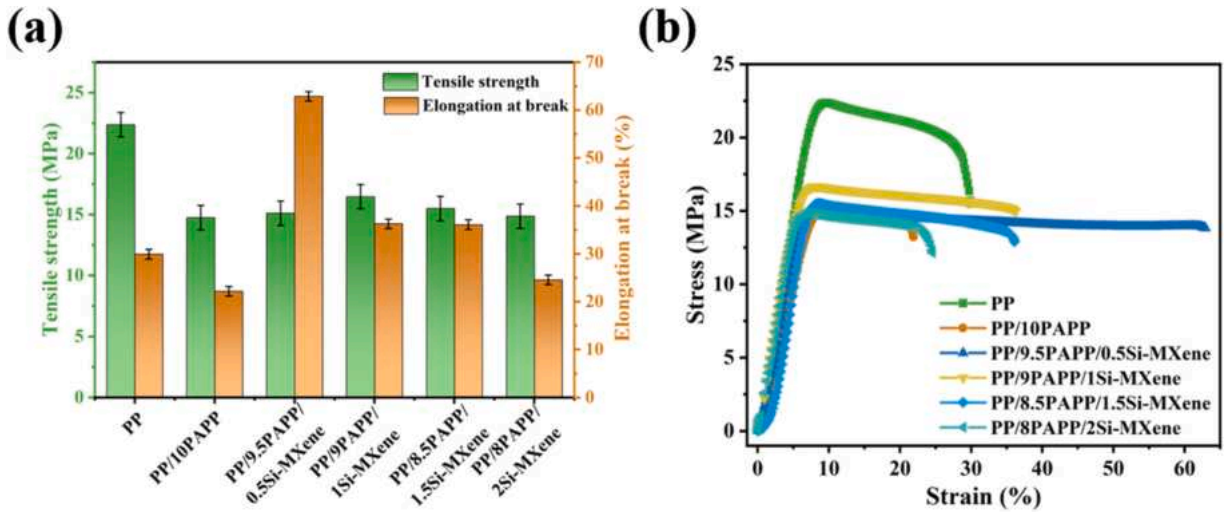

Fig. 7. Tensile properties test diagram and stress-strain curve of the PP/PAPP/Si-MXene composites with various contents.

Si-MXene aids in forming highly thermally stable graphitized carbon, creating a zigzag pathway along with the MXene's layered structure, which reduces flue gas emissions during combustion [47]. However, further increasing the Si-MXene content results in a rise in THR values for the nanocomposites, indicating that low levels of MXene enhance PAPP's effect, while higher levels may have an antagonistic effect [35].

The fire growth rate index (FIGRA), which represents the maximum ratio of HRR to burn time, is used to assess fire risk. A higher FIGRA

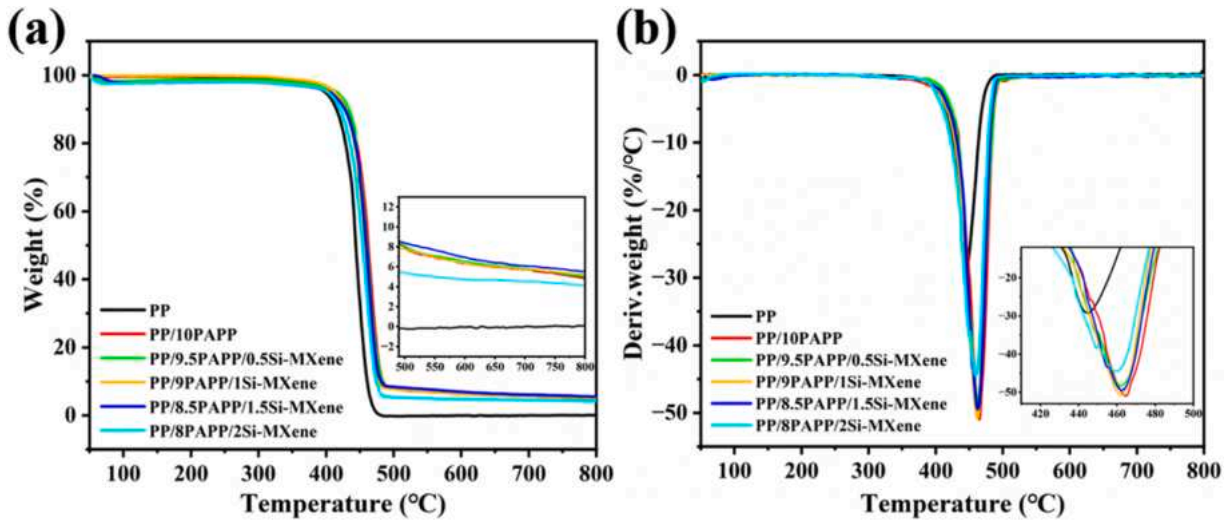

Fig. 8. (a) TGA curves and (b) DTG curves of the PP/PAPP/Si-MXene composites with various contents.

Table 3
TGA data of the PAPP/PP composites with various contents under N_2 condition.

Samples	$T_{5\ \%}$ (°C)	$T_{50\ \%}$ (°C)	T_{max} (°C)	$T_{90\ \%}$ (°C)	$Char_{800}$ (%)
PP	398.5	443.3	446.6	460.1	0.15
PP/10PAPP	410.0	461.9	464.6	483.8	4.84
PP/9.5PAPP/0.5Si-MXene	416.1	460.0	462.1	483.0	5.05
PP/9PAPP/1Si-MXene	412.9	457.9	462.2	478.4	5.24
PP/8.5PAPP/1.5Si-MXene	403.1	459.2	462.6	481.4	5.56
PP/8PAPP/2Si-MXene	402.6	453.8	459.7	473.8	4.17

value indicates a faster fire spread, whereas a lower value implies better fire safety [48]. As shown in Table 4, incorporating nanofillers results in a significant reduction in the FIGRA value, suggesting that the flame spreads more slowly in a real-world fire scenario, giving individuals more time to evacuate.

Fig. 9e shows the results of the LOI and UL-94 tests on PP composites. Pure PP exhibits rapid decomposition and combustion, leading to a significant poor performance in UL-94 rating test, i.e., NR grade, and obtains a low LOI value of 18.5 %, below the 21 % air concentration threshold. With the addition of 10 wt % PAPP, its LOI increases to 25.9 %. The incorporation of Si-MXene and PAPP results in a gradual increase in the LOI value, reaching 28.3 %, with the UL-94 test improving to V-1 grade. And real-time photos of PP, PP/10PAPP, and PP/9.5PAPP/0.5Si-MXene composites during UL-94 test are shown in **Figure S2**. All samples were ignited within 10 s of testing. At 20 s, noticeable variations emerged: the PP group exhibited intense combustion, the PP/10PAPP group showed significantly reduced flame intensity, while the flame in the PP/9.5PAPP/0.5Si-MXene group was completely extinguished. This enhanced flame retardancy is attributed to PAPP catalyzing the production of nitrogen- and phosphorus-containing compounds, while part of the MXene is oxidized to TiO_2, further promoting cross-linking and carbonization of PAPP and PP. The MXene also contributes to the formation of a high-quality carbon layer, improving its stability [49,50]. However, the addition of 2 wt % Si-MXene causes a slight decrease in the LOI to 28 %, which may be due to a reduction in the overall concentration of intumescent flame retardants. These findings highlight the importance of maintaining an optimal ratio between nanomaterials and intumescent flame retardants to avoid antagonistic interactions that could undermine flame retardancy.

3.3. Study of flame-retardant mechanism of PAPP/Si-MXene in PP composites

3.3.1. Flame-retardant mechanism in the condensed phase

Fig. 10 **(a-f)** presents digital photographs of the residual carbon after the combustion of PP and its composite materials. As shown, pure PP undergoes complete combustion, leaving no residue due to its hydrocarbon structure. The addition of 10 wt % PAPP significantly increases the residual carbon content, though its density is lower than that observed with Si-MXene incorporation. The evident expansion of the carbon residue during combustion suggests a strong synergistic effect between Si-MXene and phosphorus-nitrogen flame retardants. To further investigate the microstructure of the carbon residue, SEM analysis was performed, as shown in Fig. 10 **(b1, b2-f1, f2)**. The carbon residue of the 10 wt % PAPP sample (Fig. 10 **b1-b2**) exhibits numerous pores and gaps, likely caused by the release of non-flammable gases permeating through the carbon layer, as well as poor compatibility between the flame retardant and PP matrix. With the introduction of Si-MXene, the carbon layer becomes denser and more continuous, indicating that Si-MXene enhances the integrity of the residual carbon, effectively acting as a barrier against oxygen and heat transfer. Figs. 10**g&h** compare the carbon residue contents of PP/10PAPP and PP/8PAPP/2Si-MXene, demonstrating that the incorporation of MXene significantly increases residual carbon content. This suggests that MXene catalyzes the cross-linking of PP chain segments and the carbonization of phosphorus compounds while also facilitating phosphorus retention in the condensed phase, thereby enhancing matrix protection.

Fig. 11 (a-f) presents the XPS analysis of the chemical composition and structure of the residual carbon. The high-resolution C 1 s spectrum (Fig. 11a) for PP/10PAPP residue reveals peaks at 284.8 eV and 285.7 eV, corresponding to C–C/C–H and C–N bonds, respectively. The P 2p spectrum (Fig. 11b) exhibits peaks at 133.4 eV, 134.1 eV, and 135.0 eV, which correspond to P=O, P–O–P, and P–N–C bonds, respectively, indicating the formation of a phosphorus-containing cross-linked network that enhances the density and thermal stability of the carbon layer. Notably, the presence of Si-MXene is confirmed by the appearance of a C–Ti bond at 281.9 eV (Fig. 11c), demonstrating that PAPP and Si-MXene promote carbonization and that Si-MXene remains embedded in the residual carbon. This further supports the synergistic effect between PAPP and MXene. Figs. 11**e&f** display four characteristic peaks at 103.1 eV, 103.5 eV, 103.8 eV, and 104.4 eV, attributed to Si–O–Ti, Si–O–Si, SiO_2, and P(=O)-O-Si bonds, respectively. The Ti 2p spectrum features a peak at 456.2 eV, corresponding to Ti–O–P bonding, which contributes

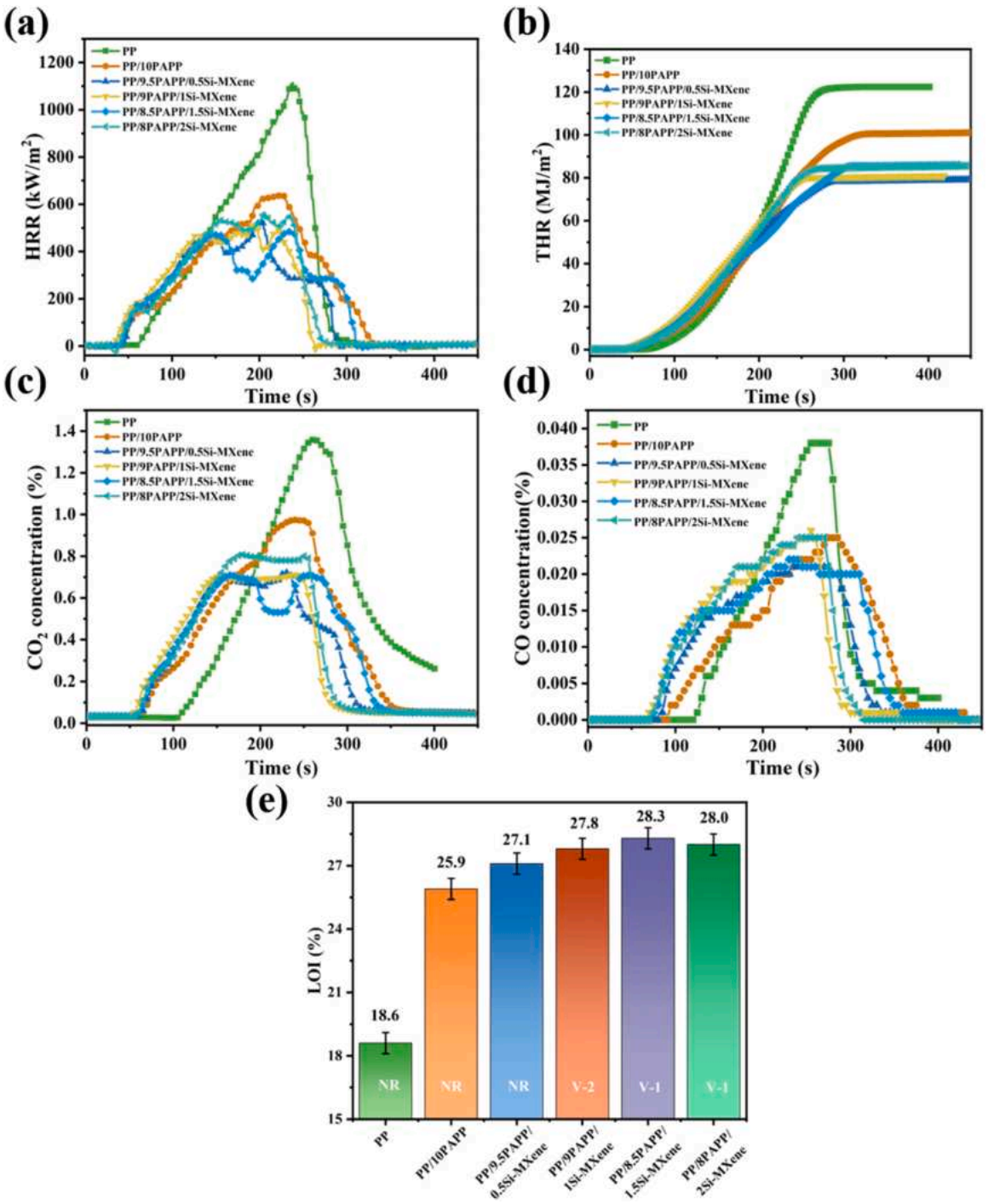

Fig. 9. (a) HRR, (b) THR, (c) CO_2 concentration, (d) CO concentration, and (e) LOI and UL-94 test results of the PP/PAPP/Si-MXene composites with various contents.

Table 4
CC test results of the PP/PAPP/Si-MXene composites with various Si-MXene mass ratios.

Samples	TTI (s)	PHRR (kW/m²)	THR (MJ/m²)	PSPR (m²/m²)	PCO (%)	PCO_2 (%)	TSP (m²)	FIGRA (Kw/m²/s)
PP	45	1113.4	122.4	6.1	0.038	1.358	6.3	4.5
PP/10PAPP	34	636.8	101.1	5.1	0.025	0.974	8.1	3.0
PP/9.5PAPP/0.5Si-MXene	35	527.4	79.1	5.0	0.021	0.721	8.2	2.6
PP/9PAPP/1Si-MXene	25	511.5	81.0	6.3	0.025	0.712	8.5	2.6
PP/8.5PAPP/1.5Si-MXene	31	485.8	85.8	5.3	0.022	0.71	9.4	2.1
PP/8PAPP/2Si-MXene	27	561.8	85.6	6.4	0.025	0.79	9.2	2.7

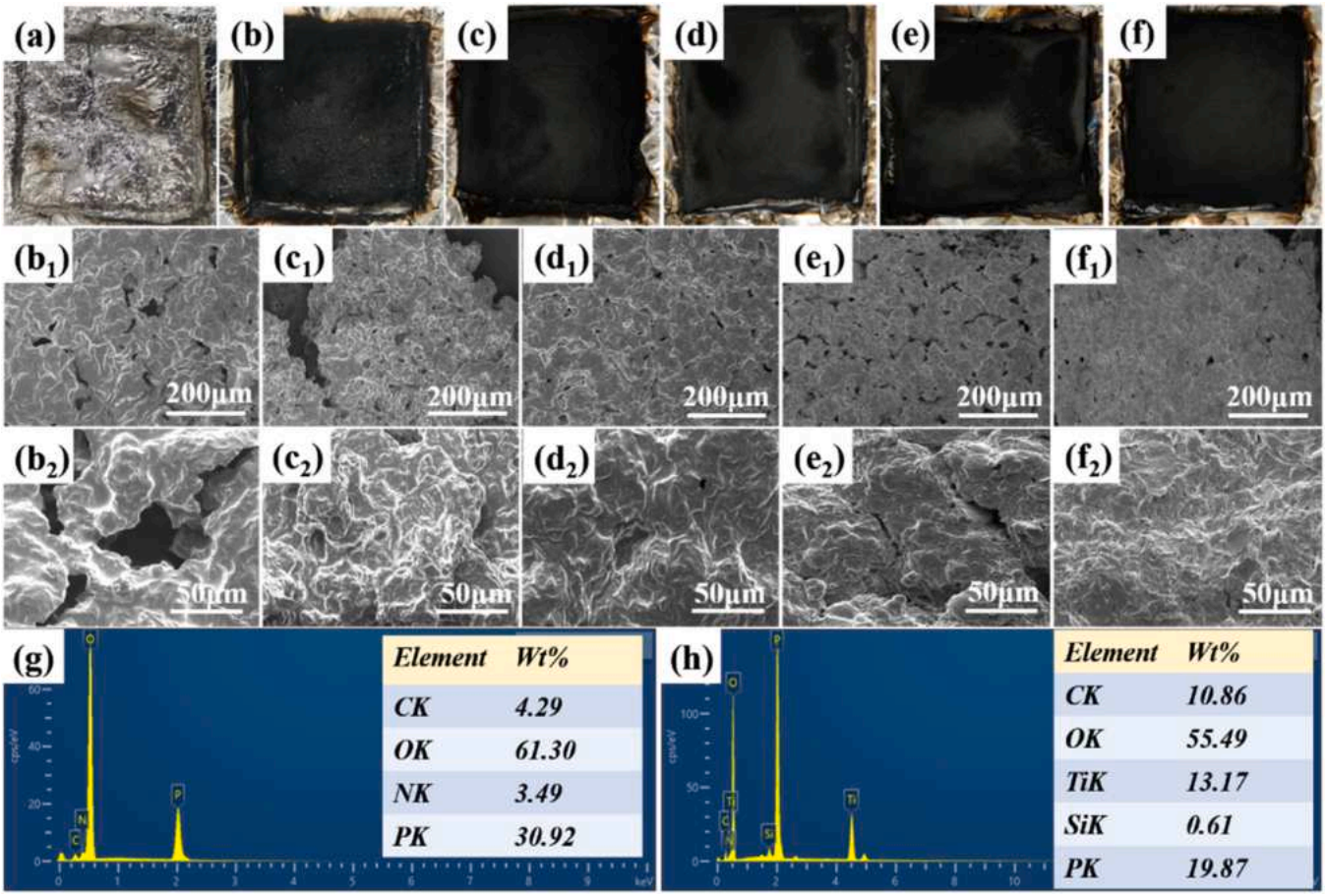

Fig. 10. (a–f) Digital photos of carbon residues of PP/PAPP/Si-MXene composites with different contents; (b1-f2) SEM images of carbon residues from PP/10PAPP, PP/9.5PAPP/0.5Si-MXene, PP/9PAPP/1Si-MXene, PP/8.5PAPP/1.5Si-MXene, and PP/8PAPP/2Si-MXene composites, respectively; (g–h) EDX images of PP/10PAPP and PP/8PAPP/2Si-MXene.

to the formation of thermally stable carbon residues [51]. Additionally, the Ti 2p spectrum reveals the presence of Ti–C, Ti^{2+}, and Ti^{3+} bonds after combustion, indicating that MXene is not fully oxidized to TiO_2 and continues to act as a catalyst, promoting the formation of a compact thermal protection layer in the residual carbon.

FTIR analysis of the residual carbon is shown in Fig. 12a. The peak in the 3430–3050 cm^{-1} range corresponds to N–H/NH_4^+ stretching vibrations, while the absorption peak at 1636 cm^{-1} is attributed to C=C bonds, suggesting that PP undergoes dehydrogenation to form graphitized structures. Peaks at 1396 cm^{-1}, 1120 cm^{-1}, 1006 cm^{-1}, and 786 cm^{-1} correspond to C–N, P–O, P–N–C, and P–O–C vibrations, respectively, confirming the participation of phosphorus-containing compounds in cross-linking carbonization. Notably, a new peak at 1076 cm^{-1}, associated with Si–O–Si stretching vibrations, suggests that silicon-containing compounds, in combination with phosphorus species and MXene, contribute to the formation of a compact thermal insulation layer during combustion test [52,53]. This mechanism inhibits the release of volatile combustion products, thereby improving flame retardancy.Fig. 12b presents XRD patterns of the residual carbon from pure PP, 10PAPP, and 8PAPP/2Si-MXene. The broad peak at 24.6° indicates a graphitized crystalline structure. In the 8PAPP/2Si-MXene system, additional peaks at 24.9°, 34.3°, and 41.9° correspond to anatase-phase TiO_2, while peaks at 28.5°, 36.6°, and 49.2° indicate rutile-phase TiO_2. A peak at 26.6° suggests the formation of TiP_2O_7 [54], likely due to the reaction between TiO_2 and phosphate during combustion. These findings confirm that MXene undergoes thermal oxidation to TiO_2, which further catalyzes the carbonization of PP, thereby improving the fire resistance of the polymer matrix.

As shown in Fig. 13, Raman spectroscopy was employed to assess the graphitic ordering in the carbon residues of PP/10PAPP and PP/8.5PAPP/1.5Si-MXene composites after the CC test. The characteristic spectral peaks of carbon materials were clearly observed at 1350 cm^{-1} (D-band, corresponding to disordered carbon structures with defects) and 1580 cm^{-1} (G-band, attributed to ordered graphitic lattices). The degree of graphitization was quantified by the integrated intensity ratio (I_D/I_G), where a lower ratio indicates higher structural ordering. Spectral fitting calculations revealed that the I_D/I_G ratio for the PP/10PAPP composite was 0.85, which decreased to 0.69 for the PP/8.5PAPP/1.5Si-MXene composite. This 18.8 % reduction in the I_D/I_G ratio demonstrates that the incorporation of Si-MXene effectively promotes the reconstruction of the carbon skeleton during pyrolysis, resulting in more ordered graphitic structures and a reduction in structural defects in the residual char.

3.3.2. *Flame-retardant mechanism in the gas phase*

TG-FTIR was then performed to characterized the gaseous products during the thermal degradation process of PP composites. As shown in Fig. 14(a-c), the primary thermal degradation of the PP composites occurs within the temperature range of 250–600 °C. Compared to pure PP, the incorporation of PAPP and Si-MXene significantly influences the pyrolysis pathway of the PP matrix. Notably, the pyrolysis behavior of PP/PAPP and PP/PAPP/Si-MXene exhibits a high degree of similarity, indicating that Si-MXene does not alter the fundamental pyrolysis mechanism of PAPP.

In addition to the typical pyrolysis products of PP, such as hydrocarbons, CO_2, and aromatic compounds, etc. the decomposition of PP/

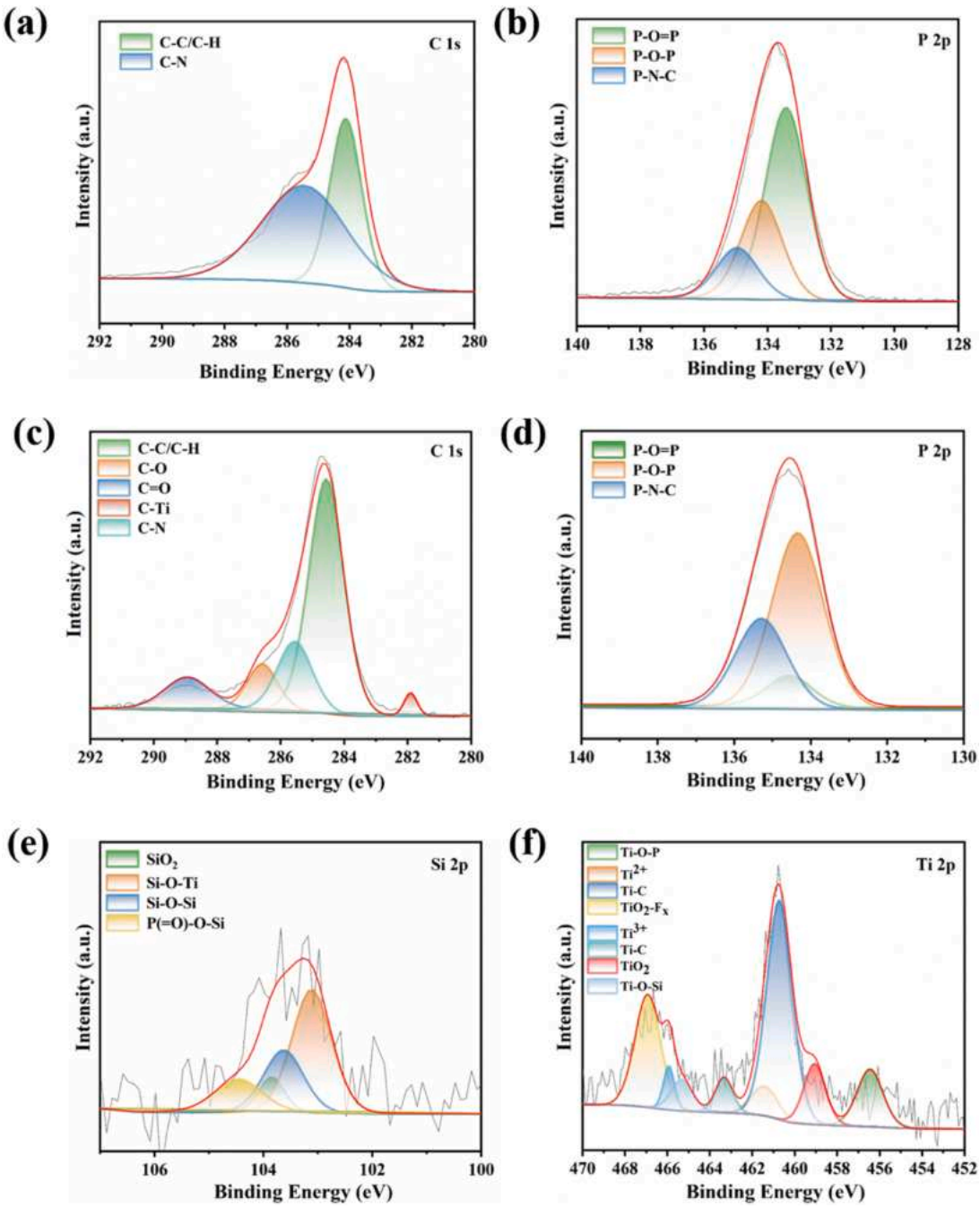

Fig. 11. (a-b) High-resolution C 1 s and P 2p XPS spectra of PP/10PAPP; (c-f) High-resolution C 1 s, P 2p, Si 2p, and Ti 2p XPS spectra of PP/9.5PAPP/0.5Si-MXene composites.

PAPP/Si-MXene composites results in the formation of new characteristic peaks corresponding to P=O, P–O–C, H_2O and NH_3. This suggests that phosphorus-containing radicals are generated during thermal decomposition, which play a critical role in capturing H· and HO· radicals, thereby suppressing combustion. Furthermore, the release of NH_3 and other inert gases helps dilute the concentration of oxygen and flammable volatiles in the gas phase. Compared to the PP/PAPP system, the hydrocarbon and CO_2 peak intensities are notably reduced in the presence of Si-MXene, further confirming the synergistic effect between Si-MXene and PAPP in flame retardancy.

Based on the combined analysis of flame-retardant effects in both the condensed and gas phases, we propose a flame-retardant mechanism for PP/PAPP/Si-MXene, as illustrated in Fig. 15. In the condensed phase, combustion leads to the formation of phosphate-containing derivatives (e.g., metaphosphates and polyphosphates) from the phosphorus-containing components of PAPP. These compounds facilitate dehydration and carbonization, cross-linking with PP molecular chains to form a stable char layer. Simultaneously, MXene undergoes partial thermal oxidation, producing TiO_2, which introduces Lewis acid sites on its surface. These sites act as solid acid catalysts, converting low-carbon pyrolysis products into highly graphitized carbon, thereby reinforcing the condensed-phase barrier effect. Moreover, the layered structure of MXene provides a physical barrier, inducing a zigzag path effect that extends the diffusion path of pyrolysis volatiles, reducing their emission and further enhancing the char's protective role. Additionally, silicon-containing compounds work synergistically with phosphorus-based compounds, increasing the cross-linking degree of the char residue and improving its flame-retardant efficiency.

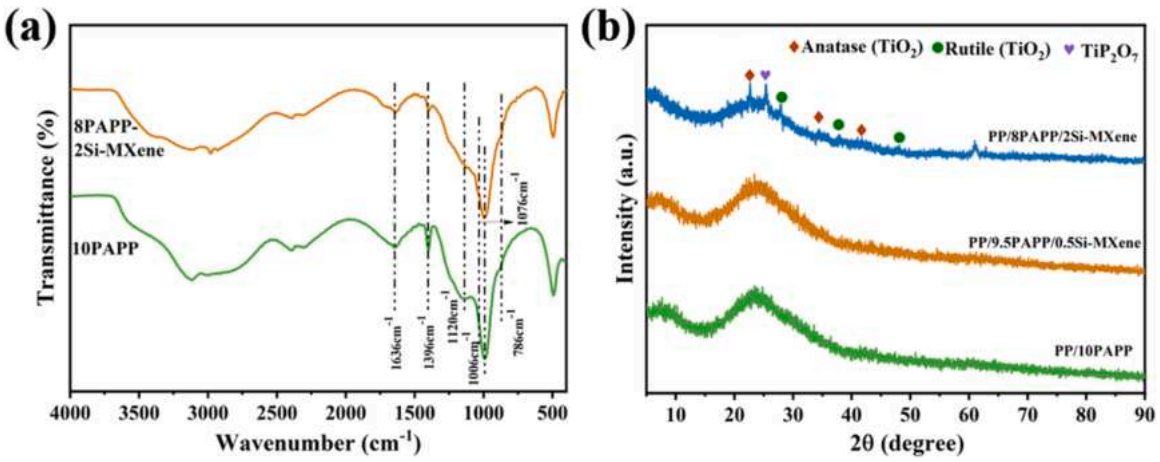

Fig. 12. (a) FTIR spectrum and (b) XRD pattern of the residual carbon.

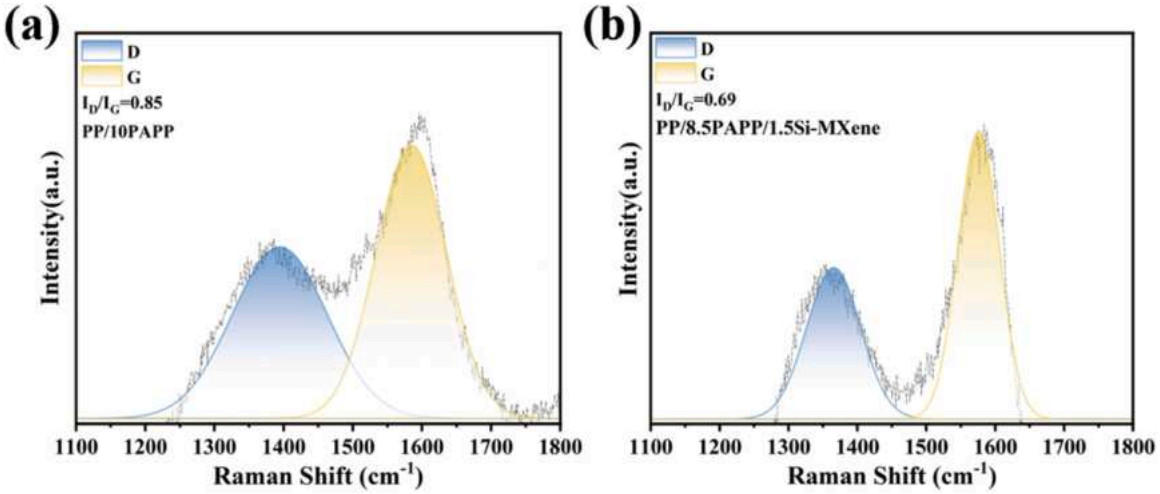

Fig. 13. Raman spectrum of char residue of (a) PP/10PAPP; (b) PP/8.5PAPP/1.5Si-Mxene obtained after CC test.

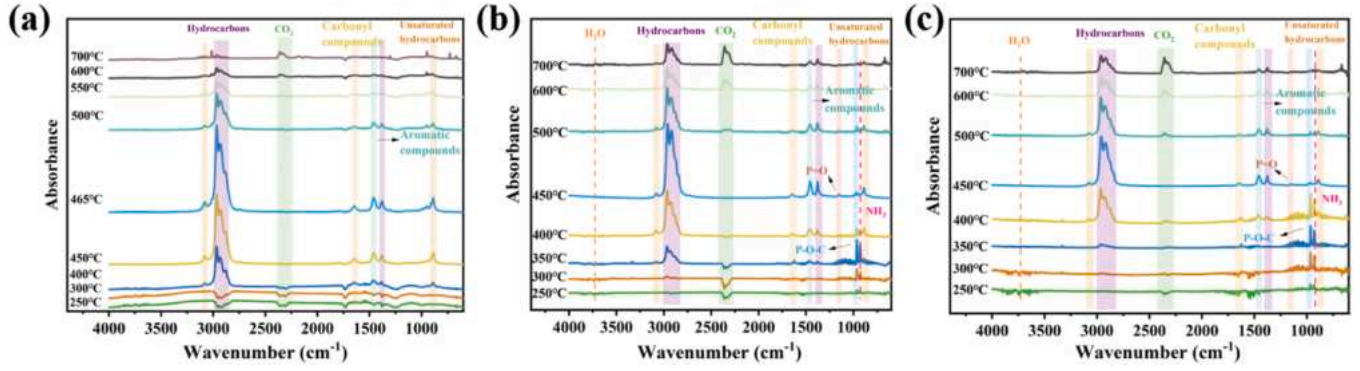

Fig. 14. FTIR spectra of pyrolysis products of the composites at different temperatures: (a) PP; (b) PP/10PAPP; (c) PP/9.5PAPP/0.5Si-MXene.

In the gas phase, the phosphorus-nitrogen components release non-flammable gases such as NH_3 and H_2O, which expand the char structure, physically isolating the underlying polymer from heat and oxygen. As combustion progresses, phosphorus compounds decompose, generating phosphorus-based free radicals (P·, PO·, PO_2·, etc.). These radicals enter the flame zone, where they effectively capture H· and HO· radicals, thereby disrupting the combustion chain reaction and terminating flame propagation. Furthermore, nitrogen-containing components decompose to release NH_3, which dilutes the concentration of flammable gases in the flame zone, ultimately reducing combustion intensity and heat release. In summary, the PP/PAPP/Si-MXene system integrates both condensed-phase and gas-phase flame-retardant mechanisms. The synergistic action of phosphorus (P), nitrogen (N), silicon (Si), and MXene nanosheets effectively reduces the combustibility of the PP matrix while simultaneously enhancing its overall flame retardancy.

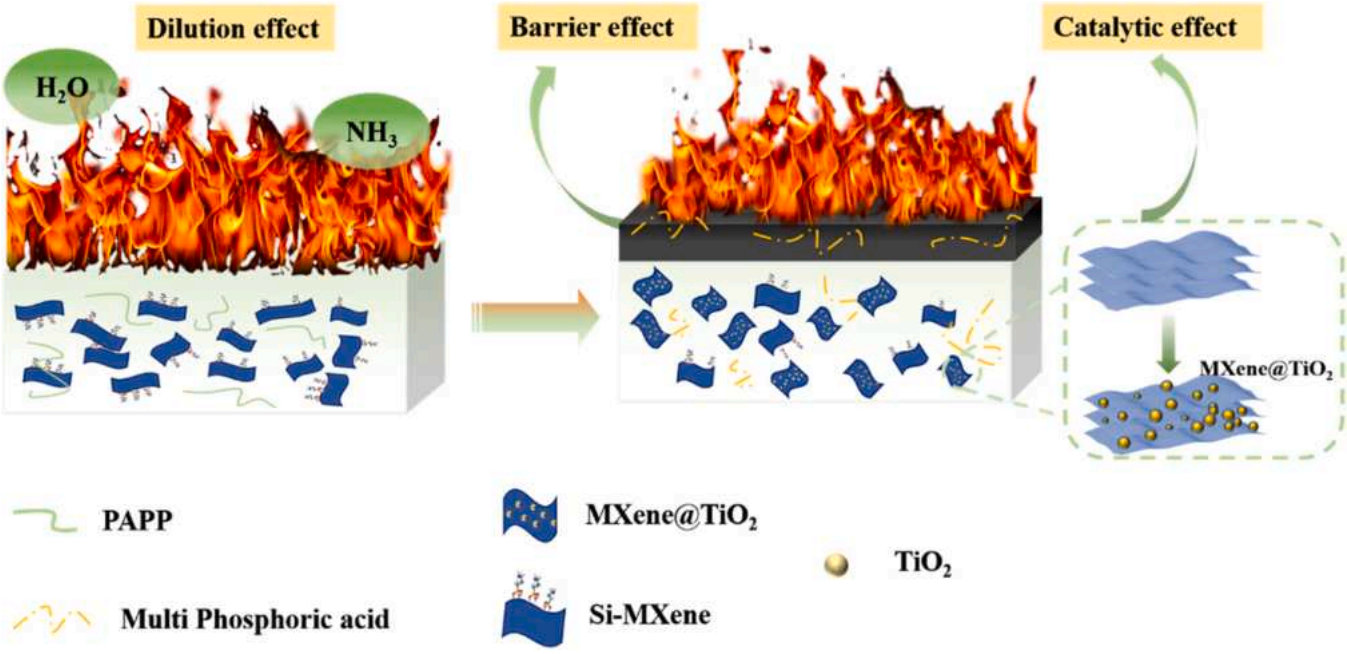

Fig. 15. Proposed flame-retardant mechanism of PAPP in combination with Si-MXene.

4. Conclusion

In this study, a PAPP/Si-MXene flame retardant system was successfully developed to enhance the fire safety performance of polypropylene (PP) composites. The synergistic effect between Si-MXene and PAPP was systematically investigated, providing insights into its condensed-phase and gas-phase flame-retardant mechanisms. The incorporation of Si-MXene significantly enhanced the flame retardancy of PP composites, leading to a 52.6 % reduction in PHRR and a 35.4 % decrease in THR at an optimal loading of 0.5 wt % Si-MXene. Investigation proves that the combination of Si-MXene and PAPP promoted the formation of a compact and graphitized char layer, acting as a thermal barrier to slow heat and mass transfer. In addition, Si-MXene catalyzed the cross-linking of phosphate compounds, enhancing the structural integrity of the char, and the presence of Si-MXene further suppressed hydrocarbon release, reinforcing the gas-phase flame-retardant effect. While in the gas phase phosphorus-containing radicals (P·, PO·, PO_2·) will be released during decomposition effectively scavenged H· and HO· radicals, thereby inhibiting flame propagation. And the decomposition of PAPP can generate NH_3 and H_2O, which acted as diluting gases, reducing the concentration of combustible species and enhancing fire resistance. This study highlights Si-MXene as an efficient nanofiller to improve the flame-retardant performance of PP composites, offering a synergistic effect with phosphorus-based flame retardants. The findings provide a promising strategy for designing high-performance, environmentally friendly flame-retardant polymers, with potential applications in automotive, electronics, and construction industries.

Declaration of generative AI and AI-assisted technologies in the writing process

During the preparation of this work the authors used ChatGPT solely to improve language and readability. After using this tool, the authors reviewed and edited the content as needed and take full responsibility for the content of the publication.

CRediT authorship contribution statement

Qinling Liu: Writing – original draft, Investigation. **Junhan Chu:** Writing – original draft, Investigation, Data curation. **Yuhui Xie:** Writing – review & editing, Supervision, Resources, Methodology, Funding acquisition. **Zhaoyu Li:** Validation, Investigation. **Feng Wu:** Writing – review & editing, Validation, Resources, Investigation. **Dong Feng:** Writing – review & editing, Validation, Resources. **Yang Meng:** Writing – review & editing, Investigation. **Yi Mei:** Writing – review & editing, Funding acquisition. **Delong Xie:** Writing – review & editing, Project administration, Funding acquisition.

Declaration of competing interest

The authors declare that they have no known competing financial interests or personal relationships that could have appeared to influence the work reported in this paper.

Acknowledgments

The authors are grateful for financial support from the National Natural Science Foundation of China (No. 22268025), the Key Research and Development Program of Yunnan Province (202403AA080003), the Special Fund for Science and Technology Innovation and Development of Xishuangbanna Prefecture (202401005), Yunnan Provincial Key Laboratory of Energy Saving in Phosphorus Chemical Engineering and New Phosphorus Materials (202205AG070067) and Yunnan Technological Innovation Center of Phosphorus Resources (202305AK340002).

Supplementary materials

Supplementary material associated with this article can be found, in the online version, at doi:10.1016/j.polymdegradstab.2025.111376.

Data availability

Data will be made available on request.

References

[1] R. Watanabe, H. Hagihara, H. Sato, Structure-property relationships of polypropylene-based nanocomposites obtained by dispersing mesoporous silica

into hydroxyl-functionalized polypropylene. Part 1: toughness, stiffness and transparency, Polym. J. 50 (11) (2018) 1057–1065.
[2] Z. Guezzout, A. Boublia, N. Haddaoui, Enhancing thermal and mechanical properties of polypropylene-nitrile butadiene rubber nanocomposites through graphene oxide functionalization, J. Polym. Res. 30 (6) (2023) 16.
[3] A.K. Maurya, G. Manik, Advances towards development of industrially relevant short natural fiber reinforced and hybridized polypropylene composites for various industrial applications: a review, J. Polym. Res. 30 (1) (2023) 20.
[4] Q.T.H. Shubhra, A. Alam, M.A. Quaiyyum, Mechanical properties of polypropylene composites: a review, J. Thermoplast. Compos. Mater. 26 (3) (2013) 362–391.
[5] M.T. Hossain, M.A. Shahid, N. Mahmud, A. Habib, M.M. Rana, S.A. Khan, M. D. Hossain, Research and application of polypropylene: a review, Discov. Nano. 19 (1) (2024) 21.
[6] W.J. Zhao, C.K. Kundu, Z.W. Li, X.H. Li, Z.J. Zhang, Flame retardant treatments for polypropylene: strategies and recent advances, Compos. Pt. A-Appl. Sci. Manuf. 145 (2021) 26.
[7] S. Bellayer, M. Dilger, S. Duquesne, M. Jimenez, Flame-retardants for polypropylene: a review, Polym. Degrad. Stabil. 230 (2024) 13.
[8] Y. Li, L.J. Qi, Y.F. Liu, J.J. Qiao, M.T. Wang, X.Y. Liu, S.S. Li, Recent advances in halogen-free flame retardants for polyolefin cable sheath materials, Polymers (Basel) 14 (14) (2022) 40.
[9] K. Wazarkar, M. Kathalewar, A. Sabnis, Reactive modification of thermoplastic and thermoset polymers using flame retardants: an overview, Polym.-Plast. Technol. Eng. 55 (1) (2016) 71–91.
[10] S. Bourbigot, S. Duquesne, Fire retardant polymers: recent developments and opportunities, J. Mater. Chem. 17 (22) (2007) 2283–2300.
[11] C.J. Zhu, M.S. He, Y. Liu, J.G. Cui, Q.L. Tai, L. Song, Y. Hu, Synthesis and application of a mono-component intumescent flame retardant for polypropylene, Polym. Degrad. Stabil. 151 (2018) 144–151.
[12] M. Yu, T.T. Zhang, J. Li, J.H. Tan, X.B. Zhu, Synthesis of a multifunctional phosphorus/silicon flame retardant via an industrial feasible technology, ACS Sustain. Chem. Eng. 11 (32) (2023) 11965–11977.
[13] C. Cheng, Y. Wang, Y.L. Lu, S.J. Li, H. Li, J. Yan, S.G. Du, Bio-based arginine surface-modified ammonium polyphosphate: an efficient intumescent flame retardant for epoxy resin, RSC Adv 12 (15) (2022) 9223–9237.
[14] Y.R. Li, Y.M. Li, W.J. Hu, D.Y. Wang, Cobalt ions loaded polydopamine nanospheres to construct ammonium polyphosphate for the improvement of flame retardancy of thermoplastic polyurethane elastomer, Polym. Degrad. Stabil. 202 (2022) 9.
[15] S.Y. Ding, P. Liu, S.M. Zhang, C. Gao, F. Wang, Y.F. Ding, M.S. Yang, Crosslinking of β-cyclodextrin and combining with ammonium polyphosphate for flame-retardant polypropylene, J. Appl. Polym. Sci. 137 (4) (2020) 12.
[16] P.L. Zheng, H.H. Zhao, J.W. Li, Q.Y. Liu, X.L. Yang, Y.M. Zhou, Enhance the fire safety of epoxy resin using ammonium polyphosphate flame retardant with the sandwich structure containing catalytic carbon formation function, J. Appl. Polym. Sci. 141 (26) (2024) 13.
[17] Z. Huang, B. Ruan, J. Wu, N. Ma, T. Jiang, F.C. Tsai, High-efficiency ammonium polyphosphate intumescent encapsulated polypropylene flame retardant, J. Appl. Polym. Sci. 138 (20) (2021) 11.
[18] Z.B. Shao, C. Deng, Y. Tan, L. Yu, M.J. Chen, L. Chen, Y.Z. Wang, Ammonium polyphosphate chemically-modified with ethanolamine as an efficient intumescent flame retardant for polypropylene, J. Mater. Chem. A 2 (34) (2014) 13955–13965.
[19] W. Tang, L.J. Qian, S.G. Prolongo, D.Y. Wang, Small core of piperazine/silane aggregation initiate efficient charring flame retardant effect in polypropylene composites, Polym. Degrad. Stabil. 208 (2023) 10.
[20] S.F. Liao, C. Deng, S.C. Huang, J.Y. Cao, Y.Z. Wang, An efficient halogen-free flame retardant for polyethylene: piperazine-modified ammonium polyphosphates with different structures, Chin. J. Polym. Sci. 34 (11) (2016) 1339–1353.
[21] W. Tang, L.J. Qian, Y.J. Chen, Y. Qiu, B. Xu, Intumescent flame retardant behavior of charring agents with different aggregation of piperazine/triazine groups in polypropylene, Polym. Degrad. Stabil. 169 (2019) 10.
[22] Y.Y. Gao, C. Deng, Y.Y. Du, S.C. Huang, Y.Z. Wang, A novel bio-based flame retardant for polypropylene from phytic acid, Polym. Degrad. Stabil. 161 (2019) 298–308.
[23] S.Z. Li, L.J. Qian, W. Tang, Y. Qiu, J.Y. Wang, W. Xi, Y.J. Chen, X. Wu, Microparticle-aggregation effect of intumescent flame retardants on flame retardancy and toughening property of polypropylene, Polym. Degrad. Stabil. 222 (2024) 12.
[24] B. Yu, X. Wang, X.D. Qian, W.Y. Xing, H.Y. Yang, L.Y. Ma, Y. Lin, S.H. Jiang, L. Song, Y. Hu, S.M. Lo, Functionalized Graphene Oxide/Phosphoramide Oligomer Hybrids Flame Retardant Prepared Via in Situ Polymerization for Improving the Fire Safety of Polypropylene, RSC Adv 4 (60) (2014) 31782–31794.
[25] V. Sharma, S. Agarwal, A. Mathur, S. Singhal, S. Wadhwa, Advancements in nanomaterial based flame-retardants for polymers: a comprehensive overview, J. Ind. Eng. Chem. 133 (2024) 38–52.
[26] C. Lamiel, I. Hussain, J.H. Warner, K.L. Zhang, Beyond Ti-based MXenes: a review of emerging non-Ti based metal-MXene structure, properties, and applications, Mater. Today 63 (2023) 313–338.
[27] J.A. Kumar, P. Prakash, T. Krithiga, D.J. Amarnath, J. Premkumar, N. Rajamohan, Y. Vasseghian, P. Saravanan, M. Rajasimman, Methods of synthesis, characteristics, and environmental applications of MXene: a comprehensive review, Chemosphere 286 (2022) 12.
[28] X.L. He, C.Q. Cui, Y. Chen, L. Zhang, X.X. Sheng, D.L. Xie, MXene and polymer collision: sparking the future of high-performance multifunctional coatings, Adv. Funct. Mater. (2024) 31.
[29] T. Yun, H. Kim, A. Iqbal, Y.S. Cho, G.S. Lee, M.K. Kim, S.J. Kim, D. Kim, Y. Gogotsi, S.O. Kim, C.M. Koo, Electromagnetic shielding of monolayer MXene assemblies, Adv. Mater. 32 (9) (2020) 9.
[30] Y. Liu, Y.J. Liu, X.M. Zhao, MXene Composite electromagnetic shielding materials: the latest research status, ACS Appl. Mater. Interfaces 16 (31) (2024) 41596–41615.
[31] C.R. Zhang, P.A. Zong, Z.S. Ge, Y.M. Ge, J. Zhang, Y.J. Rao, Z.G. Liu, W. Huang, MXene-based wearable thermoelectric respiration sensor, Nano Energy 118 (2023) 12.
[32] Y.T. Wang, Y.H. Wang, M. Jian, Q.T. Jiang, X.F. Li, MXene Key Composites: a new arena for gas sensors, Nano-Micro Lett. 16 (1) (2024) 42.
[33] P. Kuang, J. Low, B. Cheng, J. Yu, J. Fan, MXene-based photocatalysts, J. Mater. Sci. Technol. 56 (2020) 18–44.
[34] G. Murali, J.K.R. Modigunta, Y.H. Park, J.H. Lee, J. Rawal, S.Y. Lee, I. In, S.J. Park, A review on MXene synthesis, stability, and photocatalytic applications, ACS Nano (2022) 60.
[35] X.X. Sheng, S.H. Li, Y.F. Zhao, D.S. Zhai, L. Zhang, X. Lu, Synergistic effects of two-dimensional MXene and ammonium polyphosphate on enhancing the fire safety of polyvinyl alcohol composite aerogels, Polymers (Basel) 11 (12) (2019) 1964.
[36] S. Araby, B. Philips, Q.S. Meng, J. Ma, T. Laoui, C.H. Wang, Recent advances in carbon-based nanomaterials for flame retardant polymers and composites, Compos. Pt. B-Eng. 212 (2021) 29.
[37] Z.Q. Li, W. Li, L. Liao, J.B. Li, T. Wu, L.C. Ran, T.B. Zhao, B.S. Chen, Preparation and properties of polybutylene-terephthalate/graphene oxide in situ flame-retardant material, J. Appl. Polym. Sci. 137 (40) (2020) 10.
[38] Y. Luo, Y.H. Xie, W. Geng, G.F. Dai, X.X. Sheng, D.L. Xie, H. Wu, Y. Mei, Fabrication of thermoplastic polyurethane with functionalized MXene towards high mechanical strength, flame-retardant, and smoke suppression properties, J. Colloid Interface Sci. 606 (2022) 223–235.
[39] Y. Luo, Y.H. Xie, W. Geng, J.H. Chu, H. Wu, D.L. Xie, X.X. Sheng, Y. Mei, Boosting fire safety and mechanical performance of thermoplastic polyurethane by the face-to-face two-dimensional phosphorene/MXene architecture, J. Mater. Sci. Technol. 129 (2022) 27–39.
[40] H. Jiang, Y.H. Xie, Y. Jiang, Y. Luo, X.X. Sheng, Y. Mei, D.L. Xie, Rationally assembled sandwich structure of MXene-based phosphorous flame retardant at ultra-low loading nanosheets enabling fire-safe thermoplastic polyurethane, Appl. Surf. Sci. 649 (2024) 13.
[41] H. Jiang, Y.H. Xie, R. Zhu, Y. Luo, X.X. Sheng, D.L. Xie, Y. Mei, Construction of polyphosphazene-functionalized $Ti_3C_2T_X$ with high efficient flame retardancy for epoxy and its synergetic mechanisms, Chem. Eng. J. 456 (2023) 14.
[42] Z.B. Shao, C. Deng, Y. Tan, M.J. Chen, L. Chen, Y.Z. Wang, An efficient mono-component polymeric intumescent flame retardant for polypropylene: preparation and application, ACS Appl. Mater. Interfaces 6 (10) (2014) 7363–7370.
[43] S.B. Nie, Y. Hu, L. Song, Q.L. He, D.D. Yang, H. Chen, Synergistic effect between a char forming agent (CFA) and micro encapsulated ammonium polyphosphate on the thermal and flame retardant properties of polypropylene, Polym. Adv. Technol. 19 (8) (2008) 1077–1083.
[44] R. Guo, Y.C. Fan, L.J. Wang, W. Jiang, Core-rim structured carbide MXene/SiO_2 nanoplates as an ultrathin microwave absorber, Carbon N Y 169 (2020) 214–224.
[45] A. Vannier, S. Duquesne, S. Bourbigot, A. Castrovinci, G. Camino, R. Delobel, The use of POSS as synergist in intumescent recycled poly(ethylene terephthalate), Polym. Degrad. Stabil. 93 (4) (2008) 818–826.
[46] C. Liu, W. Wu, Y.Q. Shi, F.Q. Yang, M.H. Liu, Z.X. Chen, B. Yu, Y.Z. Feng, Creating MXene/reduced graphene oxide hybrid towards highly fire safe thermoplastic polyurethane nanocomposites, Compos. Pt. B-Eng. 203 (2020) 14.
[47] B. Yu, B. Tawiah, L.Q. Wang, A.C.Y. Yuen, Z.C. Zhang, L.L. Shen, B. Lin, B. Fei, W. Yang, A. Li, S.E. Zhu, E.Z. Hu, H.D. Lu, G.H. Yeoh, Interface decoration of exfoliated MXene ultra-thin nanosheets for fire and smoke suppressions of thermoplastic polyurethane elastomer, J. Hazard. Mater. 374 (2019) 110–119.
[48] B. Schartel, T.R. Hull, Development of fire-retarded materials - interpretation of cone calorimeter data, Fire Mater 31 (5) (2007) 327–354.
[49] F. Gugumus, *Re*-examination of the thermal oxidation reactions of polymers 1. New views of an old reaction, Polym. Degrad. Stabil. 74 (2) (2001) 327–339.
[50] F. Gugumus, *Re*-examination of the thermal oxidation reactions of polymers 3. Various reactions in polyethylene and polypropylene, Polym. Degrad. Stabil. 77 (1) (2002) 147–155.
[51] S.X. Zhang, H. Liu, B. Cao, Q.Z. Zhu, P. Zhang, X. Zhang, R.J. Chen, F. Wu, B. Xu, An MXene/CNTs@P nanohybrid with stable Ti-O-P bonds for enhanced lithium ion storage, J. Mater. Chem. A 7 (38) (2019) 21766–21773.
[52] Y.C. Li, B.Q. Xue, P. Qi, X.Y. Gu, J. Sun, H.F. Li, J.Y. Lin, S. Zhang, The synergistic effect between bis(2,2,6,6-tetramethyl-4-piperidyl) sebacate and polysiloxane on the photo-aging resistance and flame retardancy of polypropylene, Compos. Pt. B-Eng. 234 (2022) 10.
[53] N. Wang, S.P. Chen, L.T. Li, Z.Y. Bai, J.B. Guo, J. Qin, X.L. Chen, R. Zhao, K. Zhang, H. Wu, An environmentally friendly nanohybrid flame retardant with outstanding flame-retardant efficiency for polypropylene, J. Phys. Chem. C 125 (9) (2021) 5185–5196.
[54] B. Friederich, A. Laachachi, M. Ferriol, M. Cochez, R. Sonnier, V. Toniazzo, D. Ruch, Investigation of fire-resistance mechanisms of the ternary system (APP/MPP/TiO_2) in PMMA, Polym. Degrad. Stabil. 97 (11) (2012) 2154–2161.